ACCOUNTS of chemical research

pubs.acs.org/accounts Article

The Landscape of Gold Nanocrystal Surface Chemistry

Published as part of the Accounts of Chemical Research special issue "Ligand and Surface Chemistry of Nanoparticles".

Katherine M. Greskovich,[†] Kelly M. Powderly,[†] Maegen M. Kincanon, Nathan B. Forney, Catherine A. Jalomo, Anita Wo, and Catherine J. Murphy*

Cite This: https://doi.org/10.1021/acs.accounts.3c00109 Read Online

CONSPECTUS: Gold nanoparticles (AuNPs) exhibit unique size- and shape-dependent properties not obtainable at the macroscale. Gold nanorods (AuNRs), with their morphology-dependent optical properties, ability to convert light to heat, and high surface-to-volume ratios, are of great interest for biosensing, medicine, and catalysis. While the gold core provides many fascinating properties, this Account focuses on AuNP soft surface coatings, which govern the interactions of nanoparticles with the local environments. Postmodification of AuNP surface chemistry can greatly alter NP colloidal stability, nano-bio interactions, and functionality. Polyelectrolyte coatings provide controllable surface-coating thickness and charge, which impact the composition of the acquired corona in biological settings. Covalent modification, in which covalently bound ligands replace the original capping layer, is often performed with thiols and disulfides due to their ability to replace native coatings. N-heterocyclic carbenes and looped peptides expand the possible functionalities of the ligand layer.

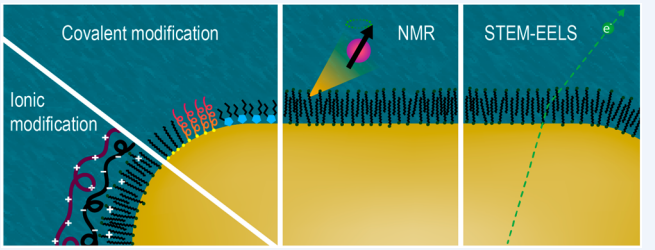

The characterization of surface ligands bound to AuNPs, in terms of ligand density and dynamics, remains a challenge. Nuclear magnetic resonance (NMR) spectroscopy is a powerful tool for understanding molecular structures and dynamics. Our recent NMR work on AuNPs demonstrated that NMR data were obtainable for ligands on NPs with diameters up to 25 nm for the first time. This was facilitated by the strong proton NMR signals of the trimethylammonium headgroup, which are present in a distinct regime from other ligand protons' signals. Ligand density analyses showed that the smallest AuNPs (below 4 nm) had the largest ligand densities, yet spin−spin T_2 measurements revealed that these smallest NPs also had the most mobile ligand headgroups. Molecular dynamics simulations were able to reconcile these seemingly contradictory results.

While NMR spectroscopy provides ligand information averaged over many NPs, the ligand distribution on individual particles' surfaces must also be probed to fully understand the surface coating. Taking advantage of improvements in electron energy loss spectroscopy (EELS) detectors employed with scanning transmission electron microscopy (STEM), a single-layer graphene substrate was used to calibrate the carbon K-edge EELS signal, allowing quantitative imaging of the carbon atom densities on AuNRs with sub-nanometer spatial resolution. In collaboration with others, we revealed that the mean value for surfactant-bilayer-coated AuNRs had 10−30% reduced ligand density at the ends of the rods compared to the sides, confirming prior indirect evidence for spatially distinct ligand densities.

Recent work has found that surface ligands on nanoparticles can, somewhat surprisingly, enhance the selectivity and efficiency of the electrocatalytic reduction of CO_2 by controlling access to the active site, tuning its electronic and chemical environment, or denying entry to impurities that poison the nanoparticle surface to facilitate reduction. Looking to the future, while NMR and EELS are powerful and complementary techniques for investigating surface coatings on AuNPs, the frontier of this field includes the development of methods to probe the surface ligands of individual NPs in a high-throughput manner, to monitor nano-bio interactions within complex matrices, and to study structure−property relationships of AuNPs in biological systems.

KEY REFERENCES

- Wu, M.; Vartanian, A. M.; Chong, G.; Pandiakumar, A. K.; Hamers, R. J.; Hernandez, R.; Murphy, C. J. Solution NMR Analysis of Ligand Environment in Quaternary Ammonium-Terminated Self-Assembled Monolayers on Gold Nanoparticles: The Effect of Surface Curvature

Received: March 3, 2023

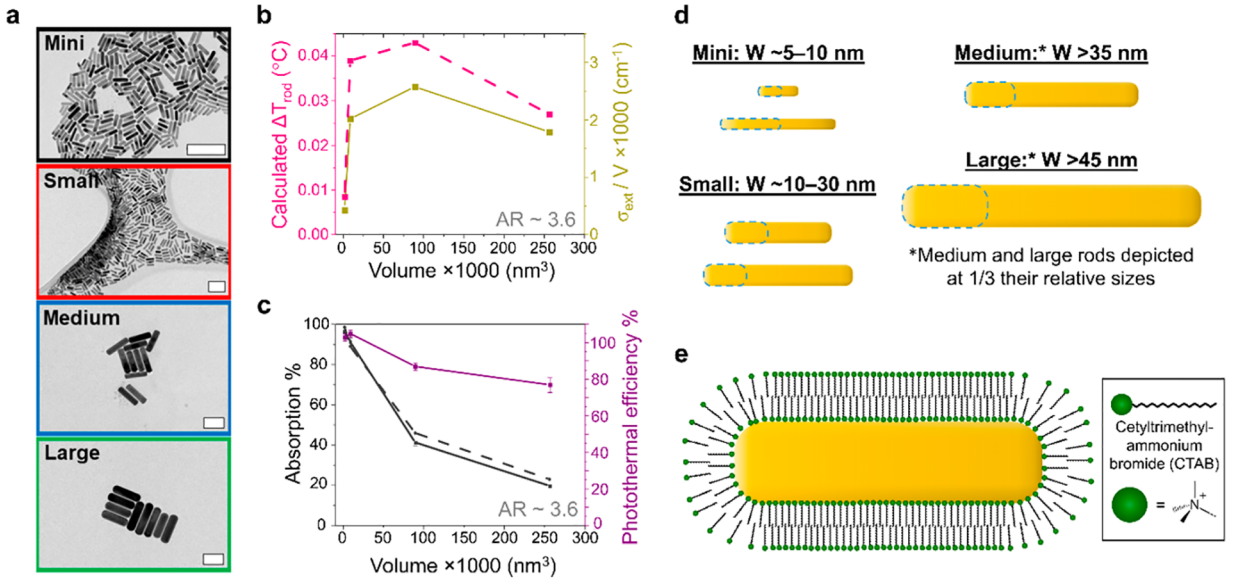

Figure 1. (a) Transmission electron micrographs of four sizes of AuNRs with an AR of 3.6. Scale bars = 100 nm. (b) Average temperature change per rod (calculated from femtosecond-laser-pulsed photothermal experiments at a given input energy, pink) and the volume-normalized extinction cross-section (gold) vs average volume of the rods. (c) Percent light absorption (left axis) determined from diffuse-reflectance spectroscopy (solid black) and electromagnetic finite element simulations (dotted black) and photothermal efficiency (right axis, purple) vs volume. (d) AuNRs of four different absolute sizes, based on their width: mini (~5–10 nm), small (~10–30 nm), medium (>35 nm), and large (>45 nm). Solid rods and dotted outlines represent the current maximum and minimum ARs, respectively, for the synthetic details in refs 18–21. (e) A bilayer of CTAB stabilizes AuNRs in aqueous solution. Reproduced in part from ref 14. Copyright 2021, American Chemical Society.

and Ligand Structure. *J. Am. Chem. Soc.* **2019**, *141*, 4316–4327.[1] Quantitative NMR analysis of both nanospheres and nanorods is utilized to characterize ligands and determine ligand density with a comparative assessment of the size dependence between nanoparticles.

Janicek, B. E.; Hinman, J. G.; Hinman, J. J.; Bae, S. h.; Wu, M.; Turner, J.; Chang, H.-H.; Park, E.; Lawless, R.; Suslick, K. S.; Murphy, C. J.; Huang, P. Y. Quantitative Imaging of Organic Ligand Density on Anisotropic Inorganic Nanocrystals. *Nano Lett.* **2019**, *19*, 6308–6314.[2] Utilization of STEM-EELS in the quantitative mapping of AuNR ligand density shows a distinct decrease in density at the ends of surfactant-capped small AuNRs while thiol-capped mini AuNRs exhibits a uniform ligand distribution.

- Hinman, J. G.; Hinman, J. J.; Janicek, B. E.; Huang, P. Y.; Suslick, K. S.; Murphy, C. J. Ultrasonic Nebulization for TEM Sample Preparation on Single-Layer Graphene Grids. *Nano Lett.* **2019**, *19*, 1938–1943.[3] Ultrasonic nebulization of aqueous AuNR samples allows for their deposition onto ultrathin support materials with minimal drying artifacts.
- Shang, H.; Wallentine, S. K.; Hofmann, D. M.; Zhu, Q.; Murphy, C. J.; Baker, L. R. Effect of surface ligands on gold nanocatalysts for CO_2 reduction. *Chem. Sci.* **2020**, *11*, 12298–12306.[4] Electrocatalytic nanoparticles show enhanced stability and selectivity to CO_2 reduction, proposed to be due to dodecanethiol surface ligand structures.

1. INTRODUCTION

Colloidal gold nanoparticles (AuNPs) have been intensely studied for applications in biological sensing, medicine, and catalysis due to their tunable optical properties, conversion of light to heat, and high surface-to-volume ratios.[5−9] It is well known that sub-visible-wavelength AuNPs display plasmons, collective coherent electron oscillations, upon appropriate excitation, with wavelengths that are tunable with NP shape and, to some extent, size.[10] Gold nanorods (AuNRs), having a short and long axis, can exhibit two plasmon modes, one corresponding to the short axis (transverse mode) and one corresponding to the long axis (longitudinal mode). The aspect ratio (AR), or length-to-width ratio, of a AuNR determines the position of the longitudinal plasmon mode.[11] This mode can thus be tuned from the visible to the near-IR (NIR), allowing excitation with wavelengths in the "water window" in which aqueous tissue absorbs little light (approximately 700–1200 nm), facilitating AuNR use in biological systems.[12]

While a AuNR's AR determines the resonant wavelength of its longitudinal plasmon band, rod volume impacts the relative absorption and scattering of resonant light, which, in concert with ensemble effects, impacts the efficiency of photothermal conversion in solution. This light-to-heat conversion is exciting for the photothermal destruction of tumors, now in human clinical trials.[13] Traditionally, smaller-volume rods have been expected to exhibit higher photothermal efficiencies as the absorption-to-scattering ratio at the resonant wavelength decreases with increasing rod volume. However, a comparison of AuNRs with identical aspect ratios but four different absolute sizes revealed that ensemble effects, such as multiple scattering of incident light, can further modify the observed photothermal properties of colloidal AuNRs in solution. Rods with widths of approximately 32 nm exhibited the largest per-particle temperature increase, and rods with an average 48-nm width hosted a higher-than-expected photothermal efficiency (Figure 1a–c).[14] Biological uptake and clearance are also impacted by the absolute dimensions of AuNRs, requiring

https://doi.org/10.1021/acs.accounts.3c00109
Acc. Chem. Res. XXXX, XXX, XXX−XXX

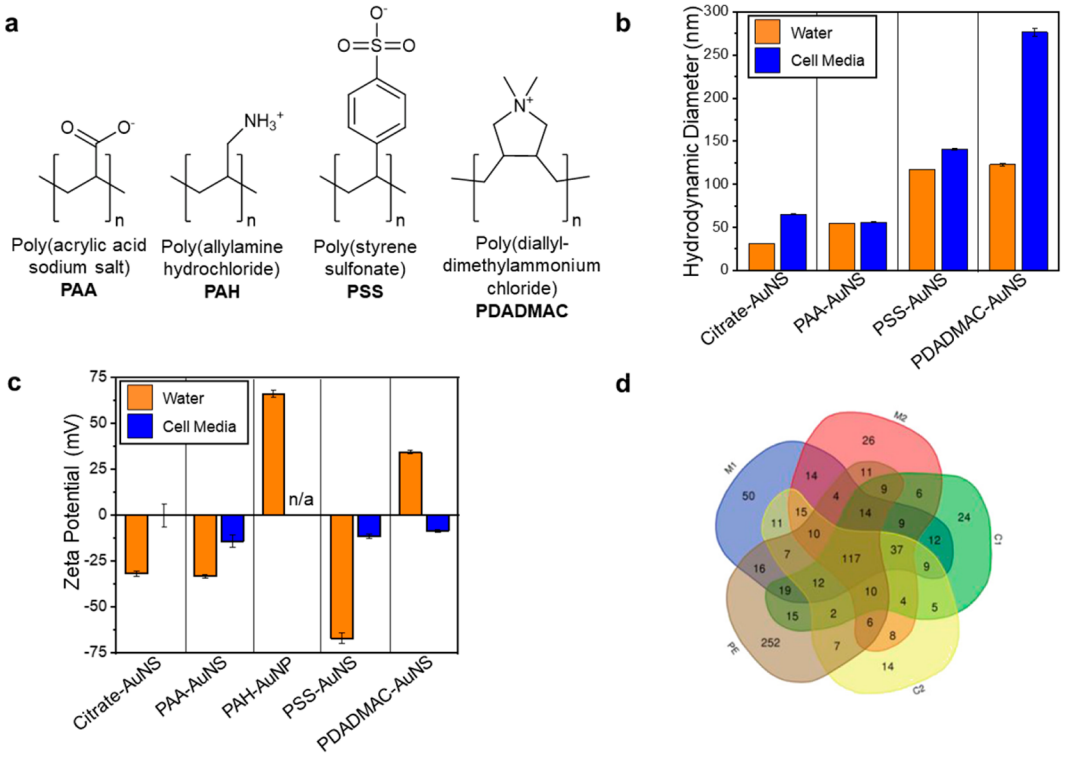

Figure 2. (a) Chemical structures of common PEs. (b) Comparison of hydrodynamic diameter for PE-wrapped AuNSs in water (orange) and in cell media (blue). (c) Comparison of ZP values for PE-wrapped AuNSs in water (orange) and cell media (blue). PAA-AuNS and PAH-AuNP were suspended in DMEM media containing FBS. PSS-AuNS and PDADMAC-AuNS were suspended in RPMI 1640 media containing FBS. Data for (b) and (c) are compiled from refs 29−31. (d) Numbers of distinct proteins discovered after NP retrieval from a total protein extract after isolation by centrifugation once or twice (C1 and C2), magnetic retrieval once or twice (M1 and M2), and that in the total protein extract (displayed as PE here). Reproduced from (d) ref 32. Copyright 2022, American Chemical Society.

consideration before implementing AuNRs in biological systems.[7,15] A general question, as far as surface chemistry goes, is to what extent the absolute size of the NPs matters for their surface chemistry, especially for dynamic soft ligand layers.

The development of shape- and size-control over colloidal AuNPs during the past 30 years offers a platform for understanding the impact of these characteristics on the ligand layers and other soft coatings that keep NPs stable in solution. The anisotropy of AuNRs is controlled by structure-directing agents, including Ag^+, Br^-, and the surfactant surface ligand cetyltrimethylammonium bromide (CTAB), which break the symmetry of the growth from the isotropic gold seeds.[16−18] Various sizes, which we have defined here by the short or transverse axis as "mini," "small," "medium," and "large" (Figure 1d), are obtained by further modifying synthesis parameters.[18−21] Along with size-controlled Au nanospheres (AuNSs), these sizes of AuNRs may allow for a systematic study of how size and curvature impact surface layers.

The as-synthesized AuNSs and AuNRs are often stabilized with citrate[22] and CTAB,[23,24] respectively. Postgrowth studies of single-crystalline AuNRs support the presence of a CTAB bilayer on the surface of the AuNRs with the hydrophilic headgroups facing the particle and the aqueous solution and the hydrophobic tails sequestered in the center (Figure 1e).[23,24] These ligand shells can be wrapped in polymers, partially or fully replaced by organic ligands that covalently bind the Au surface, or displaced during the growth of inorganic shells.[9] The modification of organic surface layers allows for tunable surface chemistry, charge, and solubility; however, characterizing the structure and composition of ligand-based surface layers remains a challenge. Herein, we describe the types of soft surface modifications, discuss advances in ligand characterization on AuNPs, offer the example of electrocatalysis as a specific application where surface ligands are noninnocent, and look ahead to the frontier of this expanding field.

2. CATEGORIES OF SOFT SURFACE COATINGS AND LIGANDS

2.1. Ionic Functionalization: Polyelectrolyte Layer-by-Layer Wrapping

To apply AuNPs in chemical and biological systems, control over the net surface charge and chemistry is vital. One way to modify the NP surface chemistry is to wrap NPs with oppositely charged polyelectrolytes (PEs; Figure 2) in a layer-by-layer approach (LbL) at appropriate ionic strengths.[25−27] In general, lower-molecular-weight (MW) PEs provide more colloidal stability for smaller NPs, while higher-MW PEs provide better stability for larger NPs. More details on synthetic considerations when applying PE coatings to NPs can be found in our previous Account.[8] Characterization methods typically utilized to monitor LbL PE coatings include extinction spectroscopy, as the plasmon band of gold is sensitive to the local refractive index out to a few nanometers; dynamic light scattering (DLS) to obtain the average hydrodynamic size in solution; and zeta potential (ZP) measurements as an estimate of net charge (Figure 2b,c).

https://doi.org/10.1021/acs.accounts.3c00109
Acc. Chem. Res. XXXX, XXX, XXX−XXX

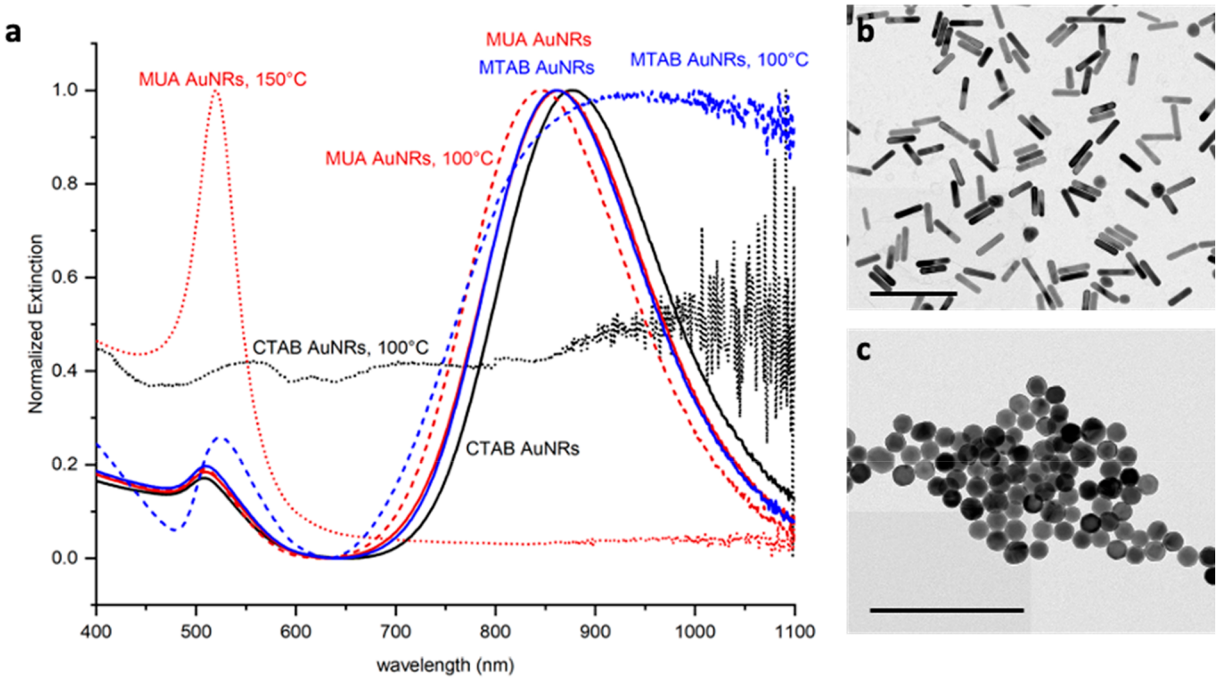

Figure 3. UV−vis extinction spectra and transmission electron microscope (TEM) images of ligand-coated AuNRs before and after heating. MUA = mercaptoundecanoic acid, MTAB = (16-mercaptohexadecayl) trimethylammonium bromide. (a) UV−vis extinction spectra of CTAB-coated AuNRs (solid black), MUA-coated AuNRs (solid red), and MTAB-coated AuNRs (solid blue) at room temperature. After heating to 100 °C, CTAB-coated AuNRs completely aggregated (dashed black), MTAB-coated rods also showed aggregation as judged by broadening and shifting of the plasmon bands (dashed blue), but MUA-coated AuNRs did not aggregate at 100 °C (dashed red). MUA-coated rods devolved into spheres as shown by the single LSPR at 150 °C (dotted red). (b) Representative TEM image of MUA-coated AuNRs after heating at 100 °C shows that MUA rods did not significantly change after heating to 100 °C. (c) TEM image of MUA-coated AuNRs transformed into spheres after heating to 150 °C. Scale bars are 200 nm.

Ultimately, the clearest picture of the success of an LbL-wrapping procedure is provided by ZP measurements (Figure 2c).

PE coatings on AuNRs can be used to confer a specific surface charge and chemistry while effectively burying the CTAB bilayer with its denaturing and cytotoxic[28] effects. As with any charged colloid, high salt concentrations will "salt out" the colloid, rendering it mostly useless for applications. To circumvent such issues for biological applications, the preincubation of PE-modified NPs in a 20% fetal bovine serum or other protein solution allows the immediate formation of a stabilizing biomolecule "corona" (Figure 2b,c).[29−31] In a biological environment, the corona can be complex, as demonstrated by a recent proteomic analysis of the corona present on gold-coated magnetic iron oxide NPs after incubation in trout gill cell extracts.[32] In this case, the original protein extract contained about 2000 proteins, identifiable by mass spectrometry (MS). When the particles were retrieved through either centrifugation or magnetic separation, each corona contained hundreds of distinct proteins, the identities of which varied with the retrieval method (Figure 2d).[32] Thus, this proteomic analysis describes the chemical history of each nanoparticle.

Even as the NP corona spontaneously forms and covers pre-established surface ligands, functionality can be engineered into the corona layer. Stordy et al. recently showed through DLS data that when incubating various NPs in a complex human blood serum, an equilibrium between corona-bound and solution proteins was established within minutes.[33] They next conjugated transferrin (Tf) to established corona proteins through *N*-hydroxysuccinimide chemistry followed by copper-free click chemistry. When these Tf-corona NPs were incubated with Tf-receptor-expressing cells in a high-protein-content medium, the corona-modified NPs were taken up by the cells at the same rate as that observed in a PBS buffer, demonstrating that the surface-bound Tf was biologically active. In contrast, Tf-PEG-NPs (PEG = poly(ethylene glycol)) exposed to the same high-protein content serum showed up to a 55% decrease in cellular uptake.[33] This work suggests that the established corona, with its modified functionality, is not buried in the presence of additional proteins and can serve as a biocompatible platform compared to organic ligands such as PEG.

2.2. Covalent Functionalization

While the above approach layers PE ligands onto existing AuNR coatings, direct attachment of ligands to the AuNP surface is most commonly done with thiols.[34] On flat gold surfaces, thiols form the quintessential self-assembled monolayer (SAM).[35] Compared to more readily desorbable ligands, thiols can impart improved colloidal stability to gold NPs. In the case of as-made CTAB-coated AuNRs, heating a solution rapidly leads to NP aggregation and precipitation, as the outer leaflet of the CTAB presumably desorbs, uncovering the underlying hydrophobic underlayer. With a thiol coating, thermal stability is greatly increased (Figure 3).

Thiol-terminated methoxy poly(ethylene glycol) (mPEG-SH) is a common polymeric thiol used to replace the initial CTAB coating on AuNRs due to its water solubility and biocompatibility. A typical exchange reaction involves the incubation of 1.0−4.0 nM AuNRs and 0.5 mM mPEG-SH

https://doi.org/10.1021/acs.accounts.3c00109
Acc. Chem. Res. XXXX, XXX, XXX−XXX

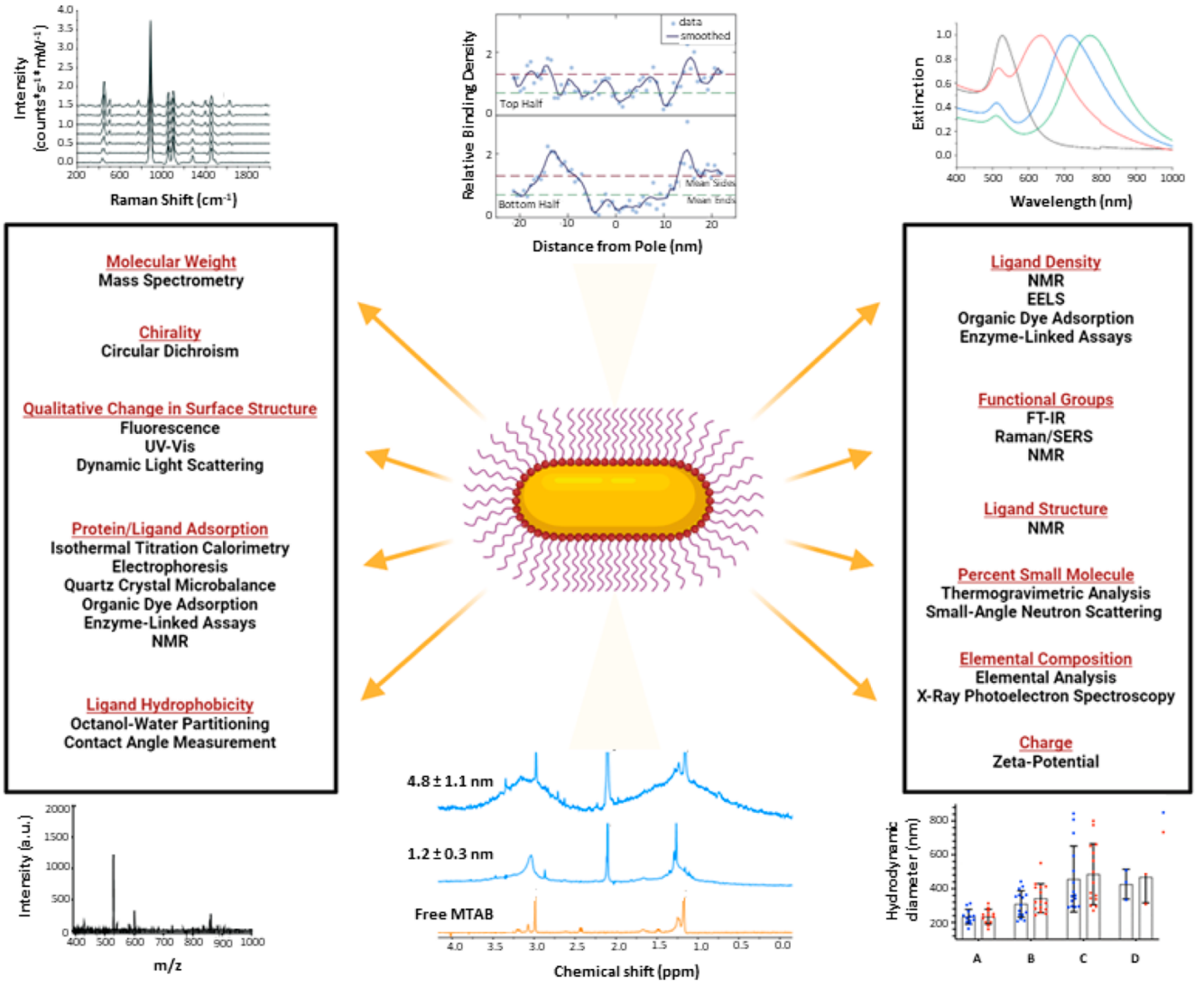

Figure 4. Analytical techniques for studying NP ligands either off-NP or on-NP. NMR and MS require the use of internal standards of known concentrations. Examples of spectral data readouts included for Raman (top left),[40] EELS (top center),[1] UV−vis (top right),[4] MS (bottom left),[58] NMR (bottom center),[4] and DLS (bottom right).[32] Spectral images reproduced from refs 40, 4, 1, 65, and 32, respectively. Copyright 2019 (refs 4 and 1,), and 2015 (ref 65), and 2022 (ref 32), American Chemical Society. Copyright 2022 (ref 40), Royal Society of Chemistry.

overnight followed by centrifugation and redispersion in water. ZP measurements before and after the ligand exchange confirm that the surface charge changes from positive (CTAB-coated AuNRs) to nearly neutral (PEG-coated AuNRs). However, some quantifications of PEG ligand density postexchange suggest that PEG may not completely replace the CTAB bilayer.[36] The oxidation of high-MW mPEG-SH results in a bulky disulfide, which somewhat unexpectedly binds with some preference to the ends of AuNRs, as judged by subsequent inorganic nanomaterial deposition solely on the sides of the AuNRs.[37,38] This sterically controlled reaction can produce anisotropic nanostructures that are of interest for catalysis or sensing.[39,40]

Nonthiol-based ligands are also capable of binding to AuNPs through Au−P, Au−N, and Au−C bonds.[41] Electrochemical reduction of diazonium ligands to an aryl or alkyl ligand allows for Au−C bond formation.[42] This Au−C bond is strong, with a binding energy (317.1 kJ/mol) that is more than twice that of Au−S (154.4 kJ/mol) and Au−NH (153.6 kJ/mol).[43] A different class of carbene ligands, N-heterocyclic carbenes (NHCs), is expanded upon in the next section.

2.3. Expanding Ligand Types on Gold Nanoparticles

2.3.1. Harnessing σ-Donating, π-Bonding, and van der Waals Effects in *N*-Heterocyclic Carbenes. While thiols are a popular choice to cap AuNPs, these ligands are still susceptible to desorption from gold when faced with extreme temperatures, pH changes, light, electrochemical stimulation, or competing exogenous thiols.[34] NHCs, which are known to strongly stabilize noble metals with simultaneous σ-donating and π-accepting properties,[44] have been shown within the last 15 years to form SAMs on both gold surfaces[45] and NPs[46] with stronger binding energies and greater resistance to the above stimuli compared to those of thiol ligands. Still under debate is the lability of the Au−C bond and the NHC-bound Au atom movement on NP surfaces, the degree of increased stability of preformed Au-NHC complexes to NP surfaces as opposed to free carbenes,[47] and the optimization of gold-NHC bonding

https://doi.org/10.1021/acs.accounts.3c00109
Acc. Chem. Res. XXXX, XXX, XXX−XXX

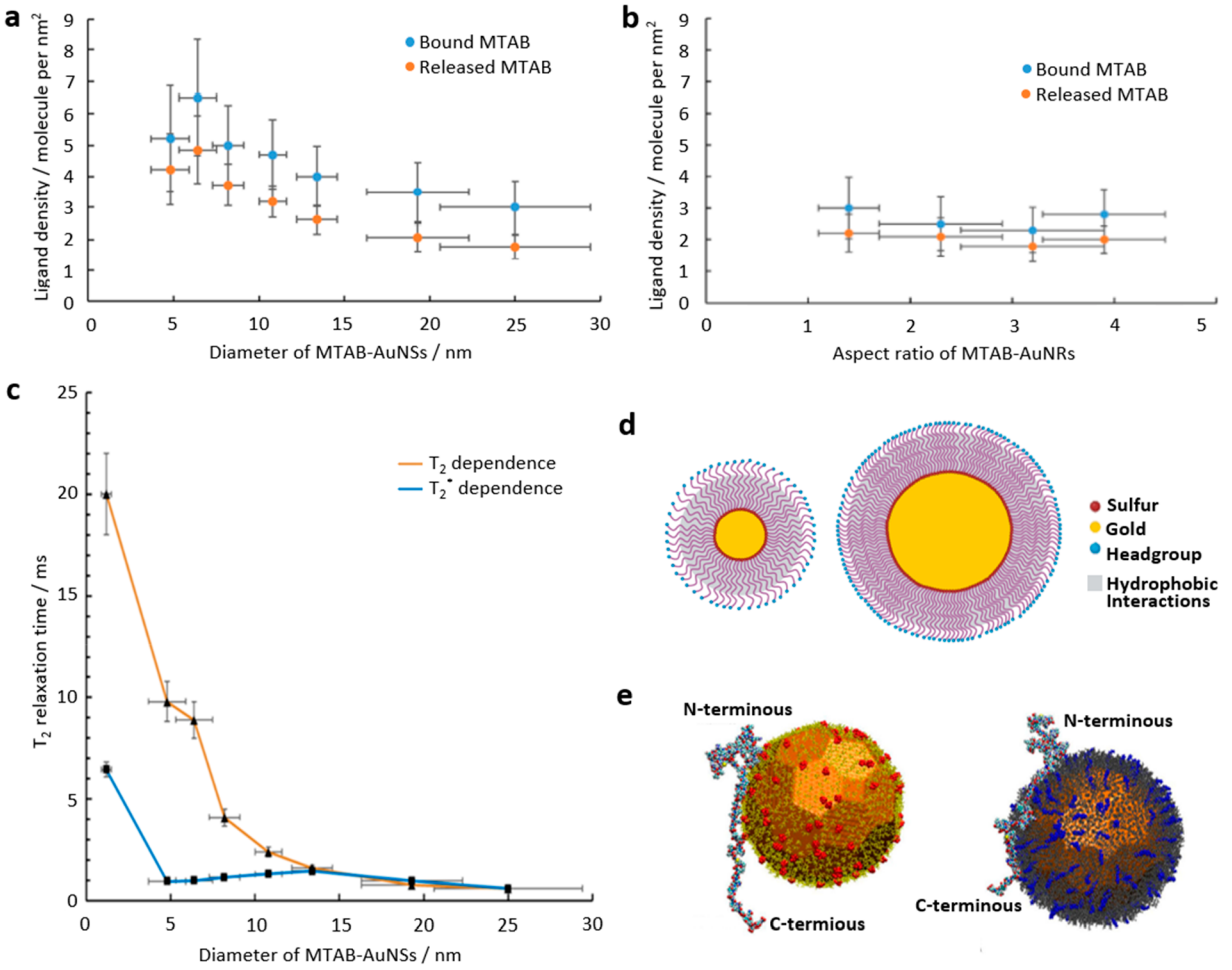

Figure 5. (a) Ligand density of MTAB bound to AuNSs as a function of AuNP diameter, measured both on-particle (bound) and after extraction (released) with reference to an internal NMR standard. (b) Ligand density for MTAB bound to AuNRs as a function of AuNR AR, measured both on-particle (bound) and after extraction (released) with reference to an internal NMR standard. (c) Dependence of T_2 (from CPMG pulse sequence) and T_2* (from peak broadening) of the MTAB headgroup protons as a function of AuNP diameter. (d) Comparative visualization of ligand conformation and packing as a function of both particle and headgroup sizes. (e) α-Synuclein simulated interaction with anionic citrate-capped AuNPs (left) and cationic MTAB-capped NPs (right). Reproduced from (a−c) ref 4 and (e) ref 60. Copyrights 2019 and 2015, respectively, American Chemical Society.

and other stabilizing forces (e.g., van der Waals interactions) to provide the most inert NP surfaces.[46,48]

2.3.2. From Protein Coronas to Peptide Display. While the native protein corona that forms around an NP in a biological fluid can be incredibly complex (Figure 2d), engineering peptides with specific functions onto NP surfaces offers another avenue to tune the chemistry and subsequent function of NPs.[49,50] Modifying the AuNP surface with peptides often involves thiol chemistry, where a covalent Au−S bond is formed through a single cysteine residue.[51]

Recently, Yan et al. have developed artificial antibodies, dubbed the "gold-body", where looped peptides are covalently attached to the AuNP surface through terminating cysteine residues.[52] The peptide design and attachment style can reduce the degree of peptide flexibility, thereby restricting peptide conformation. As a result, these looped peptides on AuNPs may more closely resemble their conformations in their native state. In the reported work, the peptide loop span was tuned by adjusting the ligand density to achieve its biologically active conformation. Contrasted with the same peptide sequence attached to the AuNP surface via monothiol ligand attachment, the looped peptide display on AuNPs demonstrated stronger binding affinity and more specificity to their targeted protein.[52]

In addition to UV−vis, DLS, and ZP measurements, the physicochemical properties of the peptide-conjugated AuNPs are commonly characterized with Fourier transform infrared spectroscopy (FTIR). Peaks associated with amide I, II, and III absorption on FTIR spectra are noted as proof of peptide attachment to the AuNP surface.[53] Other surface and elemental analysis, such as atomic force microscopy[54] and X-ray photoelectron spectroscopy,[55] have also been used to probe the surface environment on the AuNP. Mass spectrometry and amino acid analysis can provide an average estimate of the number of peptides per AuNP.[51] Quantifying unbound ligands remaining in the supernatant offers a mass balance approach to obtaining a similar result.[51,56,57] In combination, these analytical techniques can provide evidence of successful peptide conjugation to the AuNP surface. Nevertheless, robust data showing the density and packing of peptides on the AuNP surface are lacking and perhaps can be addressed with nuclear magnetic resonance (NMR) spectroscopy and scanning-transmission electron microscopy−electron

https://doi.org/10.1021/acs.accounts.3c00109
Acc. Chem. Res. XXXX, XXX, XXX−XXX

energy loss spectroscopy (STEM-EELS) characterization as discussed below.

3. ADVANCED CHARACTERIZATION METHODS FOR LIGAND DENSITY AND LIGAND DYNAMICS ON NANOPARTICLES

To better understand the true surface landscape of NPs, characterization of the quantity and distribution of ligands on the NP surface is needed. Due to their low average atomic weight, organic ligands are incredibly difficult to image with electron microscopy unless stained with a contrast agent. The number of analytical techniques used to characterize surface coatings on NPs is continuously advancing (Figure 4). Most notably, our laboratory has recently utilized nuclear magnetic resonance (NMR) spectroscopy for bulk characterization of the average ligand density and electron energy loss spectroscopy (EELS) for single-particle analysis of the heterogeneity of surface ligand density.

3.1. NMR for the Characterization of Nanoparticle Surface Functionalization

Traditionally, AuNP surface ligands are quantified through MS methods that require detaching the ligand from the NP. This method is utilized by Jiang et al. for the quantification of the number of ligands after etching with I_2 to dissolve gold[58] and by Smith et al., who quantified ligands via NMR and inductively coupled plasma−MS analysis following ligand exchange.[59] While these procedures provide powerful tools for quantifying the amount of ligand, they cannot probe on-particle ligand dynamics, ligand−ligand interactions, or ligand orientations. These on-NP properties may be probed by NMR, which provides a nondestructive method for measuring the ligand structure, orientation, and density through chemical shift, intensity, peak width, and 2D signal correlations.

Quantitative ^{1}H NMR can measure the packing density of ligands on NPs through the use of a nonoverlapping internal standard as long as NP concentrations are at approximately micromolar concentrations, so that ligand concentrations approach millimolar concentrations without aggregation. Our group was the first to successfully demonstrate this on NPs larger than 8 nm, analyzing the ligand density of gold nanospheres (AuNSs) with diameters of between 1.2 and 25 nm and mini-AuNRs with ARs from 1.4 to 3.9.[4] A (16-mercaptohexadecyl)trimethylammonium bromide (MTAB) ligand was utilized due to the trimethylammonium headgroup's unique chemical shift and the headgroup's location relatively far from the NP surface. Knowing the concentration and dimension of the NPs, average per-particle ligand densities were calculated with accuracy comparable to that of thermogravimetric analysis or MS methods. Values of 5−7 MTAB ligands/nm^2 were obtained for the smallest NPs, while values of ∼2 MTAB ligands/nm^2 were obtained for the larger NPs and the minirods (Figure 5a,b).[4] Moreover, the chemical shift of the headgroups trended downfield with increasing NP size, suggesting that larger NPs had more crowded ligand headgroups.[4]

A major value of NMR is its ability to perform pump−probe experiments to obtain dynamic information. In the case of MTAB on AuNSs and NRs, both spheres and rods, T_2 spin−spin relaxation measurements showed, surprisingly, that the smallest NPs had the most mobile headgroups while larger NPs and the minirods all had smaller T_2 values and therefore headgroups with reduced mobility (Figure 5c).[1] By pairing NMR with molecular dynamics simulations, new insights emerged: for the smallest NPs, the high curvature allowed for more ligands to bind per area, but the van der Waals interchain contacts were weak, not extending all the way to the headgroups, leading to ligand headgroup floppiness. For larger NPs, van der Waals interchain contacts were able to be accessed through the full length of the alkyl chain, leading to a much more rigid surface and, beyond a 10 nm NS diameter, very similar ligand densities due to jamming headgroups (Figure 5d).[4]

In the absence of unique NMR signals, it is possible to determine the molecular orientation on NPs if isotopic analogs are used. One example is the protein α-synuclein, labeled with ^{13}C and ^{15}N atoms.[60] 2D NMR experiments showed the loss of certain amino acid signals when bound to AuNPs of one anionic surface chemistry; this was interpreted as those signals being lost due to extreme broadening from residues close to the NP surface. Thus, a crude measure of protein orientation on NPs could be gained.[60] Changing the surface charge from negative to positive inverted the protein orientation, demonstrating that control of the initial NP surface chemistry can control protein orientation. These NMR results were confirmed by molecular dynamics simulations, where in this case the N-terminus of the protein was buried at the anionic NP surface and the C-terminus was buried at the cationic NP surface (Figure 5e).[60]

There are major challenges with NMR experiments on colloidal NPs. Probing NPs via NMR is limited by substantial line broadening, which can hinder the ability to detect surface ligands if they are too short and close to the NP surface, and low signal sensitivity, which requires approximately 100× more-concentrated samples than typical colloidal solutions, risking the aggregation of NPs. However, the favorable attributes of NMR far outweigh the practical challenges, spurring further work in this area.

3.2. EELS for the Characterization of the Surface Ligand Density Distribution

In the years leading up to 2019, end-selective adsorption of PEG-disulfide,[61] preferential linking of AuNRs,[62,63] and molecular dynamics simulations[64] offered indirect evidence for the hypothesis that the CTAB bilayer was less dense at the ends of AuNRs. In 2019, the first quantitative evidence of anisotropic ligand density on CTAB-coated AuNRs was presented through STEM-EELS mapping, which allowed the direct visualization and quantification of organic ligand density at the soft−hard interface of AuNRs.[1]

For quantitative measurements, a single-layer graphene substrate was used as an internal standard and low-background substrate.[65,66] These single-atomic-layer grids are very fragile and rupture under drop-cast sample preparation techniques. To mitigate this problem, ultrasonic nebulization was used to deposit the samples onto the graphene substrate in micrometer-scale droplets.[2] Once sample preparation was completed, EELS spectral imaging was performed to produce 2D maps of select elements surrounding the AuNR. By investigating the carbon K-edge at every point around the AuNR, we were able to map the binding density as a function of position on the surface by overlaying the ligand distribution on a simple geometric model of a AuNR.[1]

EELS mapping was performed on MTAB-capped mini (31 ± 5 nm × 11 ± 1 nm) AuNRs and CTAB-capped small (45 ± 5 nm × 15 ± 2 nm) AuNRs. The mean binding density for

https://doi.org/10.1021/acs.accounts.3c00109
Acc. Chem. Res. XXXX, XXX, XXX−XXX

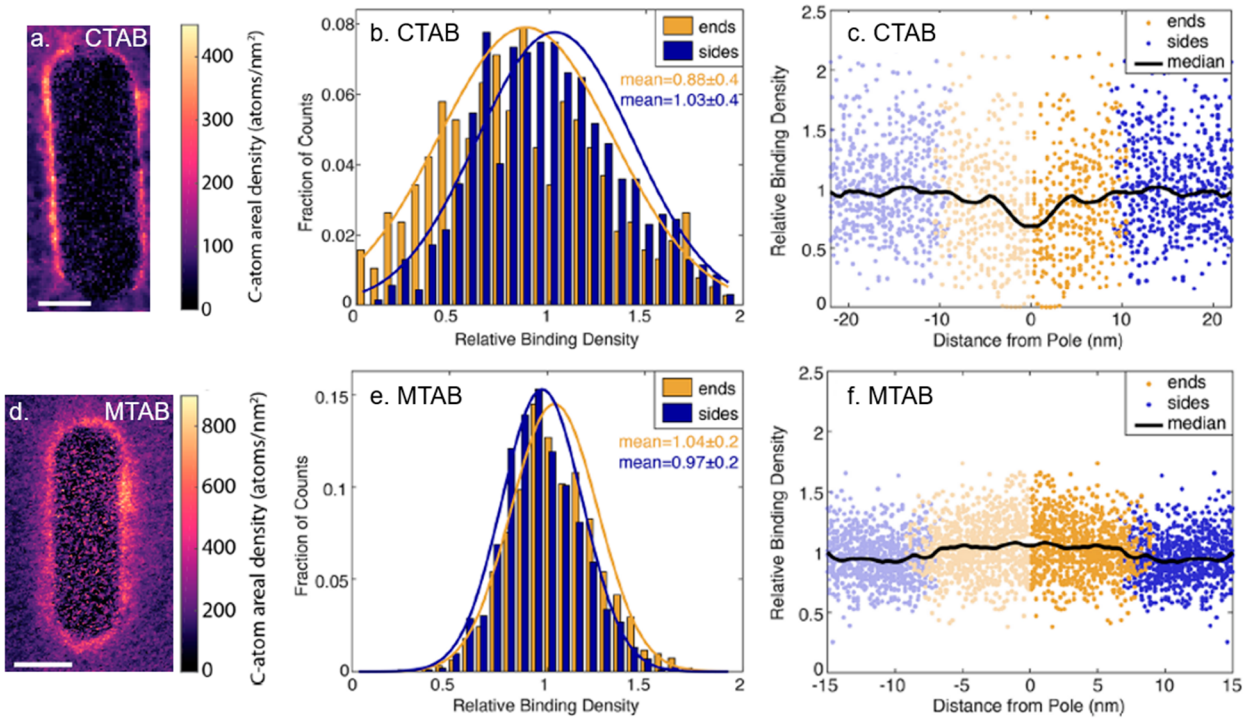

Figure 6. EELS mapping data of CTAB and MTAB AuNRs. (a) EELS carbon composition map of a CTAB-capped small AuNR. (b) Normalized histogram of the CTAB-capped small AuNR ligand binding density. The mean value at the ends is 10% lower than at the sides. (c) Plot of the CTAB-capped small AuNR relative binding density as a function of position. The anisotropy with the CTAB coating is shown by the decrease in density at the ends of the NRs. (d) EELS carbon composition map of an MTAB-capped miniature AuNR. (e) Normalized histogram of the MTAB-capped miniature AuNR binding density. The mean value for the ends and the sides are the same within error. (f) Plot of the MTAB-capped miniature AuNRs' relative binding density as a function of position. The MTAB coating shows a slight increase in density at the ends of the NR. Reproduced from ref 1. Copyright 2019, American Chemical Society.

MTAB-capped mini AuNRs and CTAB-capped small AuNRs was 3.6 ± 1 and 0.9 ± 0.2 molecules/nm^2, respectively, in agreement with previous studies.[4,67] In addition, the nature of the EELS maps allowed a separate analysis of the binding density of the ligands at the ends and sides of the NR. The normalized population-averaged ligand density measurements are visualized in Figure 6. EELS maps of CTAB-capped AuNRs showed an average 10% (maximum 30%) decrease in ligand density at the ends when compared to that on the sides (Figure 6a–c). Meanwhile, the mean value for the MTAB-capped AuNRs' relative binding density was the same within error (Figure 6d–f).[1] These data provide direct evidence to support the anisotropic distribution of CTAB on the surface of AuNRs, demonstrating the potential of quantitative EELS for investigating the heterogeneity of surface ligand layers on NPs.

4. UNEXPECTED BENEFITS OF LIGANDS ON ELECTROCATALYTICALLY ACTIVE NANOPARTICLES

The surface ligand identity, density, and possible anisotropic characteristics may impact the electrocatalytic properties of AuNPs in solution, an area studied by our group in collaboration with Baker and co-workers. Ultrasmall (<3 nm diameter) AuNPs, bound to oxide surfaces and stripped of ligands, show catalytic activity, most famously for CO oxidation[68] but also now for CO_2 reduction.[69−71] Traditionally, electrocatalytic NPs were attached to a surface and heated to remove ligands, which were generally considered to block access to the metal active site. However, an increasing number of reports show that the surface ligands on an immobilized colloidal NP can improve its catalytic activity. The current understanding of possible mechanisms is described in detail in a recent Perspective.[72]

One example of this catalytic enhancement is our study of 2-nm AuNPs capped with dodecanethiol (DDT) and immobilized on a glassy carbon electrode, which yielded a catalyst for CO_2 electroreduction that was superior to the same sample in which the DDT ligands had been removed.[3] One proposed explanation is that the DDT ligand layer selectively allows CO_2 to pass through to the NP surface while preventing the deposition of metal ions that poison active sites. In a different system, Kim et al.[73] and Yu et al.[74] have coined the term "NOLI," or "nanoparticle/ordered ligand interlayer," for systems where the surface ligands may serve a similar role as the pocket of an enzyme, controlling access to the active site and modifying the geometry and chemical environment of the reactant. Careful modifications of the surface ligand layer may yield additional improvements in catalytic efficiency and selectivity on NPs.

5. CONCLUSIONS AND FUTURE DIRECTIONS

In this Account, we have discussed various organic AuNP ligand types and efforts made to characterize those ligands in the bulk and individually, as AuNP ligands impact the NPs' biological and catalytic activity. To push the field of NP surface characterization forward, we suggest the following lines of future work.

https://doi.org/10.1021/acs.accounts.3c00109
Acc. Chem. Res. XXXX, XXX, XXX−XXX

5.1. High-Throughput Single-NP Analysis

NMR and EELS characterization methods offer insight into the average and individual ligand densities on AuNPs, respectively, but each suffers from practical challenges. We believe that the development of a high-throughput method to analyze the ligands on many NPs in quick succession will fill many gaps in knowledge about NP ligand shells. Ideally, such a technique would indicate the ligand density and orientation at many points on individual NPs, allowing for a holistic snapshot of the inhomogeneities possible in the NP surface ligand layer. Advances in tomographic reconstruction in cryo-EM may be instructive for NP ligand experiments. Single-particle ICP−MS at present can provide information about the metallic cores but not organic shells; development of work in this area would be welcome.

5.2. Monitoring NP Ligand Composition and Dynamics in Complex Matrixes

While some groups have investigated NP ligand dynamics in solution, few groups have investigated AuNP changes spatially and temporally within a complex matrix such as a biological system. Because the plasmons of gold interfere with typical fluorescence measurements, we see great promise in the continued advancement of super-resolution techniques that surpass the diffraction limit to answer these questions,[75] particularly super-resolution Raman scattering. For example, because plasmonic AuNPs lead to the SERS effect when struck by incident light, de Albuquerque and Schultz[76] tracked peptide-functionalized AuNP movement through colon cells with a wide-field super-resolution Raman spectrometer. Continued research in this area might include monitoring the change in Raman peak signals for a given suspected particle, suggesting dynamic ligand changes on the NP itself in a spatial and temporal manner.

5.3. Utilizing Combinatorial NP Libraries to Determine Structure−Function Relationships in Biological Settings

The combinatorial library is widely used to determine structure−function relationships in bioactive small-molecule research but is less commonly used to draw conclusions among different NP factors, such as core material, size, and surface chemistry and their (bio)environment. In 2018, Xu et al. studied *in vitro* and *in vivo* biological effects with a library of 21 AuNP types while systematically varying 3 NP parameters,[77] and recently, Boehnke et al. screened a library of 35 organic NPs with 488 cancer cell lines simultaneously and used multiomic data to identify genes associated with NP−cell interactions.[78] We believe that combining biological NP studies with library-type systems and omics data analysis will allow for increased clarity of the biological fate of NPs.

5.4. Final Thoughts

Overall, the enormous application space of AuNPs, from catalysis to the photothermal destruction of tumors, would greatly benefit from an increased understanding of the dynamic surface chemistry of the soft, stabilizing layers on NP surfaces, how the surface evolves over time, and how best the surface can be engineered at the front end for maximum beneficial impact.

AUTHOR INFORMATION

Corresponding Author

Catherine J. Murphy − *Department of Chemistry, University of Illinois Urbana−Champaign, Urbana, Illinois 61801, United States*; orcid.org/0000-0001-7066-5575; Email: murphycj@illinois.edu

Authors

Katherine M. Greskovich − *Department of Chemistry, University of Illinois Urbana−Champaign, Urbana, Illinois 61801, United States*

Kelly M. Powderly − *Department of Chemistry, University of Illinois Urbana−Champaign, Urbana, Illinois 61801, United States*

Maegen M. Kincanon − *Department of Chemistry, University of Illinois Urbana−Champaign, Urbana, Illinois 61801, United States*

Nathan B. Forney − *Department of Chemistry, University of Illinois Urbana−Champaign, Urbana, Illinois 61801, United States*

Catherine A. Jalomo − *Department of Chemistry, University of Illinois Urbana−Champaign, Urbana, Illinois 61801, United States*

Anita Wo − *Department of Chemistry, University of Illinois Urbana−Champaign, Urbana, Illinois 61801, United States*

Complete contact information is available at: https://pubs.acs.org/10.1021/acs.accounts.3c00109

Author Contributions

†K.M.G. and K.M.P. made equal contributions to this work.

Notes

The authors declare no competing financial interest.

Biographies

Katherine M. Greskovich obtained her B.S. degree in chemistry with a biochemistry concentration from Kent State University in 2019 with a minor in writing. She is currently a Ph.D. candidate in the Murphy group at UIUC. Her research focuses on the study of NHC-based ligands on gold nanoparticles.

Kelly M. Powderly obtained her Ph.D. in chemistry and materials science from Princeton University in 2022, where she synthesized and characterized magnetic materials. Now, she is a postdoctoral research associate in the Murphy laboratory at UIUC harnessing plasmonic properties of gold nanorods interfacing with inorganic solids.

Maegen M. Kincanon received her B.S. degree in professional chemistry from the University of Evansville in Indiana in 2019, with minors in ethics, biology, and environmental studies. She is currently a Ph.D. candidate in the Murphy group at UIUC. Her research focuses on the self-assembly of gold nanorods and the use of gold nanoparticles for drug delivery.

Nathan B. Forney is a chemistry Ph.D. student in the Murphy group at UIUC. He received his B.S. in chemistry and biochemistry and molecular biology from Otterbein University in 2020. His research interests include quantitative EELS mapping of organic ligands on gold nanorods.

Catherine A. Jalomo is a chemistry Ph.D. candidate and member of the Murphy and Zimmerman groups at UIUC. She received her B.S. degree in chemistry from Fresno Pacific University in 2020. Her research focuses on nanoparticles for smart delivery systems.

Anita Wo is a Ph.D. candidate in the Murphy group at UIUC. She received her B.A. degree in chemistry from Wellesley College in 2017. Her research interests include studying interactions at the nanobio interface to predict biological outcomes.

https://doi.org/10.1021/acs.accounts.3c00109
Acc. Chem. Res. XXXX, XXX, XXX−XXX

Catherine J. Murphy (B.S. chemistry, Illinois, 1986; B.S. biochemistry, Illinois, 1986; Ph.D., Wisconsin, 1990) holds the Larry R. Faulkner Endowed Chair in Chemistry at the University of Illinois at Urbana−Champaign (UIUC). After postdoctoral fellowships at the California Institute of Technology with J. K. Barton (1990−1993), she joined the faculty of chemistry and biochemistry at the University of South Carolina. After rising through the faculty ranks at South Carolina (1993−2009), she was recruited back to UIUC in 2009.

■ ACKNOWLEDGMENTS

We thank the National Science Foundation for supporting our work (CHE-2107793 and DMR-1720633). Portions of the primary work referred to in this Account were supported by the National Science Foundation under CHE-2001611, the NSF Center for Sustainable Nanotechnology.

■ REFERENCES

(1) Wu, M.; Vartanian, A. M.; Chong, G.; Pandiakumar, A. K.; Hamers, R. J.; Hernandez, R.; Murphy, C. J. Solution NMR Analysis of Ligand Environment in Quaternary Ammonium-Terminated Self-Assembled Monolayers on Gold Nanoparticles: The Effect of Surface Curvature and Ligand Structure. *J. Am. Chem. Soc.* **2019**, *141*, 4316−4327.

(2) Janicek, B. E.; Hinman, J. G.; Hinman, J. J.; Bae, S. h.; Wu, M.; Turner, J.; Chang, H.-H.; Park, E.; Lawless, R.; Suslick, K. S.; Murphy, C. J.; Huang, P. Y. Quantitative Imaging of Organic Ligand Density on Anisotropic Inorganic Nanocrystals. *Nano Lett.* **2019**, *19*, 6308−6314.

(3) Hinman, J. G.; Hinman, J. J.; Janicek, B. E.; Huang, P. Y.; Suslick, K. S.; Murphy, C. J. Ultrasonic Nebulization for TEM Sample Preparation on Single-Layer Graphene Grids. *Nano Lett.* **2019**, *19*, 1938−1943.

(4) Shang, H.; Wallentine, S. K.; Hofmann, D. M.; Zhu, Q.; Murphy, C. J.; Baker, L. R. Effect of surface ligands on gold nanocatalysts for CO_2 reduction. *Chem. Sci.* **2020**, *11*, 12298−12306.

(5) Murphy, C. J.; Gole, A. M.; Stone, J. W.; Sisco, P. N.; Alkilany, A. M.; Goldsmith, E. C.; Baxter, S. C. Gold Nanoparticles in Biology: Beyond Toxicity to Cellular Imaging. *Acc. Chem. Res.* **2008**, *41*, 1721−1730.

(6) Alkilany, A. M.; Thompson, L. B.; Boulos, S. P.; Sisco, P. N.; Murphy, C. J. Gold nanorods: Their potential for photothermal therapeutics and drug delivery, tempered by the complexity of their biological interactions. *Adv. Drug Delivery Rev.* **2012**, *64*, 190−199.

(7) Alkilany, A. M.; Lohse, S. E.; Murphy, C. J. The Gold Standard: Gold Nanoparticle Libraries To Understand the Nano−Bio Interface. *Acc. Chem. Res.* **2013**, *46*, 650−661.

(8) Murphy, C. J.; Chang, H.-H.; Falagan-Lotsch, P.; Gole, M. T.; Hofmann, D. M.; Hoang, K. N. L.; McClain, S. M.; Meyer, S. M.; Turner, J. G.; Unnikrishnan, M.; Wu, M.; Zhang, X.; Zhang, Y. Virus-Sized Gold Nanorods: Plasmonic Particles for Biology. *Acc. Chem. Res.* **2019**, *52*, 2124−2135.

(9) Han, C.; Qi, M.-Y.; Tang, Z.-R.; Gong, J.; Xu, Y.-J. Gold nanorods-based hybrids with tailored structures for photoredox catalysis: fundamental science, materials design and applications. *Nano Today* **2019**, *27*, 48−72.

(10) El-Sayed, M. A. Some Interesting Properties of Metals Confined in Time and Nanometer Space of Different Shapes. *Acc. Chem. Res.* **2001**, *34*, 257−264.

(11) Murphy, C. J.; Sau, T. K.; Gole, A. M.; Orendorff, C. J.; Gao, J.; Gou, L.; Hunyadi, S. E.; Li, T. Anisotropic Metal Nanoparticles: Synthesis, Assembly, and Optical Applications. *J. Phys. Chem. B* **2005**, *109*, 13857−13870.

(12) Huang, X.; Jain, P. K.; El-Sayed, I. H.; El-Sayed, M. A. Plasmonic photothermal therapy (PPTT) using gold nanoparticles. *Las. Med. Sci.* **2008**, *23*, 217−228.

(13) Rastinehad, A. R.; Anastos, H.; Wajswol, E.; Winoker, J. S.; Sfakianos, J. P.; Doppalapudi, S. K.; Carrick, M. R.; Knauer, C. J.; Taouli, B.; Lewis, S. C.; Tewari, A. K.; Schwartz, J. A.; Canfield, S. E.; George, A. K.; West, J. L.; Halas, N. J. Gold nanoshell-localized photothermal ablation of prostate tumors in a clinical pilot device study. *Proc. Natl. Acad. Sci. U.S.A.* **2019**, *116*, 18590−18596.

(14) Meyer, S. M.; Pettine, J.; Nesbitt, D. J.; Murphy, C. J. Size Effects in Gold Nanorod Light-to-Heat Conversion under Femtosecond Illumination. *J. Phys. Chem. C* **2021**, *125*, 16268−16278.

(15) Li, Z.; Tang, S.; Wang, B.; Li, Y.; Huang, H.; Wang, H.; Li, P.; Li, C.; Chu, P. K.; Yu, X.-F. Metabolizable Small Gold Nanorods: Size-dependent Cytotoxicity, Cell Uptake and In Vivo Biodistribution. *ACS Biomat. Sci. Eng.* **2016**, *2*, 789−797.

(16) Jana, N. R.; Gearheart, L.; Murphy, C. J. Seed-Mediated Growth Approach for Shape-Controlled Synthesis of Spheroidal and Rod-like Gold Nanoparticles Using a Surfactant Template. *Adv. Mater.* **2001**, *13*, 1389−1393.

(17) Nikoobakht, B.; El-Sayed, M. A. Preparation and Growth Mechanism of Gold Nanorods (NRs) Using Seed-Mediated Growth Method. *Chem. Mater.* **2003**, *15*, 1957−1962.

(18) Sau, T. K.; Murphy, C. J. Seeded High Yield Synthesis of Short Au Nanorods in Aqueous Solution. *Langmuir* **2004**, *20*, 6414−6420.

(19) Chang, H.-H.; Murphy, C. J. Mini Gold Nanorods with Tunable Plasmonic Peaks beyond 1000 nm. *Chem. Mater.* **2018**, *30*, 1427−1435.

(20) Vigderman, L.; Zubarev, E. R. High-Yield Synthesis of Gold Nanorods with Longitudinal SPR Peak Greater than 1200 nm Using Hydroquinone as a Reducing Agent. *Chem. Mater.* **2013**, *25*, 1450−1457.

(21) Ye, X.; Zheng, C.; Chen, J.; Gao, Y.; Murray, C. B. Using Binary Surfactant Mixtures To Simultaneously Improve the Dimensional Tunability and Monodispersity in the Seeded Growth of Gold Nanorods. *Nano Lett.* **2013**, *13*, 765−771.

(22) Turkevich, J.; Stevenson, P. C.; Hillier, J. A study of the nucleation and growth processes in the synthesis of colloidal gold. *Discuss. Faraday Soc.* **1951**, *11*, 55−75.

(23) Nikoobakht, B.; El-Sayed, M. A. Evidence for Bilayer Assembly of Cationic Surfactants on the Surface of Gold Nanorods. *Langmuir* **2001**, *17*, 6368−6374.

(24) Sau, T. K.; Murphy, C. J. Self-Assembly Patterns Formed upon Solvent Evaporation of Aqueous Cetyltrimethylammonium Bromide-Coated Gold Nanoparticles of Various Shapes. *Langmuir* **2005**, *21*, 2923−2929.

(25) Decher, G.; Hong, J. D.; Schmitt, J. Buildup of ultrathin multilayer films by a self-assembly process: III. Consecutively alternating adsorption of anionic and cationic polyelectrolytes on charged surfaces. *Thin Solid Films* **1992**, *210*−*211*, 831−835.

(26) Mayya, K. S.; Schoeler, B.; Caruso, F. Preparation and Organization of Nanoscale Polyelectrolyte-Coated Gold Nanoparticles. *Adv. Funct. Mater.* **2003**, *13*, 183−188.

(27) Gittins, D. I.; Caruso, F. Tailoring the Polyelectrolyte Coating of Metal Nanoparticles. *J. Phys. Chem. B* **2001**, *105*, 6846−6852.

(28) Alkilany, A. M.; Nagaria, P. K.; Hexel, C. R.; Shaw, T. J.; Murphy, C. J.; Wyatt, M. D. Cellular uptake and cytotoxicity of gold nanorods: molecular origin of cytotoxicity and surface effects. *Small* **2009**, *5*, 701−8.

(29) Zhang, X.; Falagan-Lotsch, P.; Murphy, C. J. Nanoparticles Interfere with Chemotaxis: An Example of Nanoparticles as Molecular "Knockouts" at the Cellular Level. *ACS Nano* **2021**, *15*, 8813−8825.

(30) Falagan-Lotsch, P.; Murphy, C. J. Network-based analysis implies critical roles of microRNAs in the long-term cellular responses to gold nanoparticles. *Nanoscale* **2020**, *12*, 21172−21187.

(31) Falagan-Lotsch, P.; Grzincic, E. M.; Murphy, C. J. One low-dose exposure of gold nanoparticles induces long-term changes in human cells. *Proc. Natl. Acad. Sci. U.S.A.* **2016**, *113*, 13318−13323.

(32) Hoang, K. N. L.; Wheeler, K. E.; Murphy, C. J. Isolation Methods Influence the Protein Corona Composition on Gold-Coated Iron Oxide Nanoparticles. *Anal. Chem.* **2022**, *94*, 4737−4746.

https://doi.org/10.1021/acs.accounts.3c00109
Acc. Chem. Res. XXXX, XXX, XXX−XXX

(33) Stordy, B.; Zhang, Y.; Sepahi, Z.; Khatami, M. H.; Kim, P. M.; Chan, W. C. W. Conjugating Ligands to an Equilibrated Nanoparticle Protein Corona Enables Cell Targeting in Serum. *Chem. Mater.* **2022**, *34*, 6868−6882.
(34) Vericat, C.; Vela, M. E.; Benitez, G.; Carro, P.; Salvarezza, R. C. Self-assembled monolayers of thiols and dithiols on gold: new challenges for a well-known system. *Chem. Soc. Rev.* **2010**, *39*, 1805−34.
(35) Nuzzo, R. G.; Allara, D. L. Adsorption of bifunctional organic disulfides on gold surfaces. *J. Am. Chem. Soc.* **1983**, *105*, 4481−4483.
(36) Hore, M. J. A.; Ye, X.; Ford, J.; Gao, Y.; Fei, J.; Wu, Q.; Rowan, S. J.; Composto, R. J.; Murray, C. B.; Hammouda, B. Probing the Structure, Composition, and Spatial Distribution of Ligands on Gold Nanorods. *Nano Lett.* **2015**, *15*, 5730−5738.
(37) Wang, F.; Cheng, S.; Bao, Z.; Wang, J. Anisotropic Overgrowth of Metal Heterostructures Induced by a Site-Selective Silica Coating. *Angew. Chem., Int. Ed.* **2013**, *52*, 10344−10348.
(38) Medeghini, F.; Pettine, J.; Meyer, S. M.; Murphy, C. J.; Nesbitt, D. J. Regulating and Directionally Controlling Electron Emission from Gold Nanorods with Silica Coatings. *Nano Lett.* **2022**, *22*, 644−651.
(39) Hoang, K. N. L.; McClain, S. M.; Meyer, S. M.; Jalomo, C. A.; Forney, N. B.; Murphy, C. J. Site-selective modification of metallic nanoparticles. *Chem. Commun.* **2022**, *58*, 9728−9741.
(40) Meyer, S. M.; Murphy, C. J. Anisotropic silica coating on gold nanorods boosts their potential as SERS sensors. *Nanoscale* **2022**, *14*, 5214−5226.
(41) Heuer-Jungemann, A.; Feliu, N.; Bakaimi, I.; Hamaly, M.; Alkilany, A.; Chakraborty, I.; Masood, A.; Casula, M. F.; Kostopoulou, A.; Oh, E.; Susumu, K.; Stewart, M. H.; Medintz, I. L.; Stratakis, E.; Parak, W. J.; Kanaras, A. G. The Role of Ligands in the Chemical Synthesis and Applications of Inorganic Nanoparticles. *Chem. Rev.* **2019**, *119*, 4819−4880.
(42) Betelu, S.; Tijunelyte, I.; Boubekeur-Lecaque, L.; Ignatiadis, I.; Ibrahim, J.; Gaboreau, S.; Berho, C.; Toury, T.; Guenin, E.; Lidgi-Guigui, N.; Félidj, N.; Rinnert, E.; Chapelle, M. L. d. l. Evidence of the Grafting Mechanisms of Diazonium Salts on Gold Nanostructures. *J. Phys. Chem. B* **2016**, *120*, 18158−18166.
(43) Sherman, L. M.; Finley, M. D.; Borsari, R. K.; Schuster-Little, N.; Strausser, S. L.; Whelan, R. J.; Jenkins, D. M.; Camden, J. P. N-Heterocyclic Carbene Ligand Stability on Gold Nanoparticles in Biological Media. *ACS Omega* **2022**, *7*, 1444−1451.
(44) Hopkinson, M. N.; Richter, C.; Schedler, M.; Glorius, F. An overview of N-heterocyclic carbenes. *Nature* **2014**, *510*, 485−496.
(45) Crudden, C. M.; Horton, J. H.; Narouz, M. R.; Li, Z.; Smith, C. A.; Munro, K.; Baddeley, C. J.; Larrea, C. R.; Drevniok, B.; Thanabalasingam, B.; McLean, A. B.; Zenkina, O. V.; Ebralidze, I. I.; She, Z.; Kraatz, H.-B.; Mosey, N. J.; Saunders, L. N.; Yagi, A. Simple direct formation of self-assembled N-heterocyclic carbene monolayers on gold and their application in biosensing. *Nat. Commun.* **2016**, *7*, 12654.
(46) Man, R. W. Y.; Li, C.-H.; MacLean, M. W. A.; Zenkina, O. V.; Zamora, M. T.; Saunders, L. N.; Rousina-Webb, A.; Nambo, M.; Crudden, C. M. Ultrastable Gold Nanoparticles Modified by Bidentate N-Heterocyclic Carbene Ligands. *J. Am. Chem. Soc.* **2018**, *140*, 1576−1579.
(47) MacLeod, M. J.; Goodman, A. J.; Ye, H.-Z.; Nguyen, H. V. T.; Van Voorhis, T.; Johnson, J. A. Robust gold nanorods stabilized by bidentate N-heterocyclic-carbene−thiolate ligands. *Nat. Chem.* **2019**, *11*, 57−63.
(48) Bélanger-Bouliga, M.; Mahious, R.; Pitroipa, P. I.; Nazemi, A. Perylene diimide-tagged N-heterocyclic carbene-stabilized gold nanoparticles: How much ligand desorbs from surface in presence of thiols? *Dalton Trans.* **2021**, *50*, 5598−5606.
(49) Tkachenko, A. G.; Xie, H.; Coleman, D.; Glomm, W.; Ryan, J.; Anderson, M. F.; Franzen, S.; Feldheim, D. L. Multifunctional Gold Nanoparticle−Peptide Complexes for Nuclear Targeting. *J. Am. Chem. Soc.* **2003**, *125*, 4700−4701.
(50) Huang, X.; Peng, X.; Wang, Y.; Wang, Y.; Shin, D. M.; El-Sayed, M. A.; Nie, S. A Reexamination of Active and Passive Tumor Targeting by Using Rod-Shaped Gold Nanocrystals and Covalently Conjugated Peptide Ligands. *ACS Nano* **2010**, *4*, 5887−5896.
(51) Lévy, R.; Thanh, N. T. K.; Doty, R. C.; Hussain, I.; Nichols, R. J.; Schiffrin, D. J.; Brust, M.; Fernig, D. G. Rational and Combinatorial Design of Peptide Capping Ligands for Gold Nanoparticles. *J. Am. Chem. Soc.* **2004**, *126*, 10076−10084.
(52) Yan, G.-H.; Wang, K.; Shao, Z.; Luo, L.; Song, Z.-M.; Chen, J.; Jin, R.; Deng, X.; Wang, H.; Cao, Z.; Liu, Y.; Cao, A. Artificial antibody created by conformational reconstruction of the complementary-determining region on gold nanoparticles. *Proc. Natl. Acad. Sci. U.S.A.* **2018**, *115*, E34−E43.
(53) Xu, X.; Liu, Y.; Yang, Y.; Wu, J.; Cao, M.; Sun, L. One-pot synthesis of functional peptide-modified gold nanoparticles for gene delivery. *Colloids Surf. A Physicochem. Eng. Asp.* **2022**, *640*, 128491.
(54) Kulkarni, T.; Mukhopadhyay, D.; Bhattacharya, S. Influence of surface moieties on nanomechanical properties of gold nanoparticles using atomic force microscopy. *Appl. Surf. Sci.* **2022**, *591*, 153175.
(55) Richter, Ł.; Stevens, C. A.; Silva, P. J.; Julià, L. R.; Malinverni, C.; Wei, L.; Łoś, M.; Stellacci, F. Peptide-Grafted Nontoxic Cyclodextrins and Nanoparticles against Bacteriophage Infections. *ACS Nano* **2022**, *16*, 18990−19001.
(56) Egorova, E. A.; Arias-Alpizar, G.; Vlieg, R. C.; Gooris, G. S.; Bouwstra, J. A.; Noort, J. v.; Kros, A.; Boyle, A. L. Coating gold nanorods with self-assembling peptide amphiphiles promotes stability and facilitates in vivo two-photon imaging. *J. Mater. Chem. B* **2022**, *10*, 1612−1622.
(57) Xu, X.; Ding, Y.; Hadianamrei, R.; Lv, S.; You, R.; Pan, F.; Zhang, P.; Wang, N.; Zhao, X. Antimicrobial peptide functionalized gold nanorods combining near-infrared photothermal therapy for effective wound healing. *Colloids Surf., B* **2022**, *220*, 112887.
(58) Jiang, Y.; Huo, S.; Mizuhara, T.; Das, R.; Lee, Y.-W.; Hou, S.; Moyano, D. F.; Duncan, B.; Liang, X.-J.; Rotello, V. M. The Interplay of Size and Surface Functionality on the Cellular Uptake of Sub-10 nm Gold Nanoparticles. *ACS Nano* **2015**, *9*, 9986−9993.
(59) Smith, A. M.; Marbella, L. E.; Johnston, K. A.; Hartmann, M. J.; Crawford, S. E.; Kozycz, L. M.; Seferos, D. S.; Millstone, J. E. Quantitative Analysis of Thiolated Ligand Exchange on Gold Nanoparticles Monitored by ^{1}H NMR Spectroscopy. *Anal. Chem.* **2015**, *87*, 2771−2778.
(60) Lin, W.; Insley, T.; Tuttle, M. D.; Zhu, L.; Berthold, D. A.; Král, P.; Rienstra, C. M.; Murphy, C. J. Control of Protein Orientation on Gold Nanoparticles. *J. Phys. Chem. C* **2015**, *119*, 21035−21043.
(61) Hinman, J. G.; Eller, J. R.; Lin, W.; Li, J.; Li, J.; Murphy, C. J. Oxidation State of Capping Agent Affects Spatial Reactivity on Gold Nanorods. *J. Am. Chem. Soc.* **2017**, *139*, 9851−9854.
(62) Caswell, K. K.; Wilson, J. N.; Bunz, U. H. F.; Murphy, C. J. Preferential End-to-End Assembly of Gold Nanorods by Biotin−Streptavidin Connectors. *J. Am. Chem. Soc.* **2003**, *125*, 13914−13915.
(63) Nie, Z.; Fava, D.; Rubinstein, M.; Kumacheva, E. Supramolecular" Assembly of Gold Nanorods End-Terminated with Polymer "Pom-Poms": Effect of Pom-Pom Structure on the Association Modes. *J. Am. Chem. Soc.* **2008**, *130*, 3683−3689.
(64) Meena, S. K.; Sulpizi, M. Understanding the Microscopic Origin of Gold Nanoparticle Anisotropic Growth from Molecular Dynamics Simulations. *Langmuir* **2013**, *29*, 14954−14961.
(65) Huang, P. Y.; Ruiz-Vargas, C. S.; van der Zande, A. M.; Whitney, W. S.; Levendorf, M. P.; Kevek, J. W.; Garg, S.; Alden, J. S.; Hustedt, C. J.; Zhu, Y.; Park, J.; McEuen, P. L.; Muller, D. A. Grains and grain boundaries in single-layer graphene atomic patchwork quilts. *Nature* **2011**, *469*, 389−392.
(66) Lee, Z.; Jeon, K.-J.; Dato, A.; Erni, R.; Richardson, T. J.; Frenklach, M.; Radmilovic, V. Direct Imaging of Soft−Hard Interfaces Enabled by Graphene. *Nano Lett.* **2009**, *9*, 3365−3369.
(67) Kawasaki, H.; Nishimura, K.; Arakawa, R. Influence of the Counterions of Cetyltrimetylammonium Salts on the Surfactant Adsorption onto Gold Surfaces and the Formation of Gold Nanoparticles. *J. Phys. Chem. C* **2007**, *111*, 2683−2690.

https://doi.org/10.1021/acs.accounts.3c00109
Acc. Chem. Res. XXXX, XXX, XXX−XXX

(68) Valden, M.; Lai, X.; Goodman, D. W. Onset of Catalytic Activity of Gold Clusters on Titania with the Appearance of Nonmetallic Properties. *Science* **1998**, *281*, 1647−1650.
(69) Chen, Y.; Li, C. W.; Kanan, M. W. Aqueous CO_2 Reduction at Very Low Overpotential on Oxide-Derived Au Nanoparticles. *J. Am. Chem. Soc.* **2012**, *134*, 19969−19972.
(70) Zhu, W.; Michalsky, R.; Metin, Ö.; Lv, H.; Guo, S.; Wright, C. J.; Sun, X.; Peterson, A. A.; Sun, S. Monodisperse Au Nanoparticles for Selective Electrocatalytic Reduction of CO_2 to CO. *J. Am. Chem. Soc.* **2013**, *135*, 16833−16836.
(71) Mistry, H.; Reske, R.; Zeng, Z.; Zhao, Z.-J.; Greeley, J.; Strasser, P.; Cuenya, B. R. Exceptional Size-Dependent Activity Enhancement in the Electroreduction of CO_2 over Au Nanoparticles. *J. Am. Chem. Soc.* **2014**, *136*, 16473−16476.
(72) Zhu, Q.; Murphy, C. J.; Baker, L. R. Opportunities for Electrocatalytic CO_2 Reduction Enabled by Surface Ligands. *J. Am. Chem. Soc.* **2022**, *144*, 2829−2840.
(73) Kim, D.; Yu, S.; Zheng, F.; Roh, I.; Li, Y.; Louisia, S.; Qi, Z.; Somorjai, G. A.; Frei, H.; Wang, L.-W.; Yang, P. Selective CO_2 electrocatalysis at the pseudocapacitive nanoparticle/ordered-ligand interlayer. *Nat. Energy* **2020**, *5*, 1032−1042.
(74) Yu, S.; Kim, D.; Qi, Z.; Louisia, S.; Li, Y.; Somorjai, G. A.; Yang, P. Nanoparticle Assembly Induced Ligand Interactions for Enhanced Electrocatalytic CO_2 Conversion. *J. Am. Chem. Soc.* **2021**, *143*, 19919−19927.
(75) Leighton, R. E.; Alperstein, A. M.; Frontiera, R. R. Label-Free Super-Resolution Imaging Techniques. *Annu. Rev. Anal. Chem.* **2022**, *15*, 37−55.
(76) de Albuquerque, C. D. L.; Schultz, Z. D. Super-resolution Surface-Enhanced Raman Scattering Imaging of Single Particles in Cells. *Anal. Chem.* **2020**, *92*, 9389−9398.
(77) Xu, M.; Soliman, M. G.; Sun, X.; Pelaz, B.; Feliu, N.; Parak, W. J.; Liu, S. How Entanglement of Different Physicochemical Properties Complicates the Prediction of in Vitro and in Vivo Interactions of Gold Nanoparticles. *ACS Nano* **2018**, *12*, 10104−10113.
(78) Boehnke, N.; Straehla, J. P.; Safford, H. C.; Kocak, M.; Rees, M. G.; Ronan, M.; Rosenberg, D.; Adelmann, C. H.; Chivukula, R. R.; Nabar, N.; Berger, A. G.; Lamson, N. G.; Cheah, J. H.; Li, H.; Roth, J. A.; Koehler, A. N.; Hammond, P. T., Massively parallel pooled screening reveals genomic determinants of nanoparticle delivery. *Science* **2022**, *377*, eabm5551. DOI: DOI: 10.1126/science.abm5551.

https://doi.org/10.1021/acs.accounts.3c00109
Acc. Chem. Res. XXXX, XXX, XXX−XXX